Available on CMS information server **CMS CR 1997/004**

CMS Conference Report

29 April 1998

Comprehensive Modeling of Silicon Microstrip Detectors

D. Passeri, P. Ciampolini, M. Baroncini

Istituto di Elettronica, Università di Perugia, Via Duranti 93, 06131 Perugia, Italy

A. Santocchia, G. M. Bilei, B. Checcucci, E. Fiandrini

INFN - Sezione di Perugia, Via A. Pascoli 1, 06100 Perugia, Italy

Abstract

In this work, the application of numerical device simulation to the analysis of high resistivity silicon microstrip detectors is illustrated. The analysis of DC, AC and transient responses of a single-sided, DC-coupled detector has been carried out, providing results in good agreement with experimental data. In particular, transient-mode simulation has been exploited to investigate the collection of charges generated by ionizing particles. To this purpose, an additional generation term has been incorporated into the transport equations; the motion of impact-generated carriers under the combined action of ohmic and diffusive forces is hence accounted for. Application to radiation tolerance studies is also introduced.

Presented at *IEEE Nuclear Science Symposium*, Los Angeles (CA), November 10, 1996

Submitted to *IEEE Transactions on Nuclear Science*

1 INTRODUCTION

The next generation of collider experiments in High Energy Physics (HEP) will be carried out on a high luminosity ($10^{33} - 10^{34}$ cm^{-2} s^{-1}) Large Hadron Collider (LHC) at CERN. The high rate and the topology of events at LHC will translate into tracking detectors that have to survive large radiation doses, have good timing resolution to resolve different beam crossing and have high position resolution as well. Silicon detectors will be extensively used in tracking systems proposed at LHC and will be suited to such an environment due to their short charge-collection time and rather good radiation tolerance. The development of silicon detectors for LHC demands large resources, both in terms of time and money. Device-simulation programs may help in the prediction of the characteristics of silicon detectors, depending upon their geometry and fabrication parameters, without actually manufacturing them. A number of open questions, mainly concerning optimization issues, are in fact still to be addressed and clarified, before starting the massive detector production. Among them, radiation tolerance deserves particular consideration: effects of bulk and surface damage can actually be included in the simulation, allowing for analyzing the detector performance after an arbitrary irradiation, and thus to evaluate its radiation-hardness characteristics.

Reduction of both optimization time and prototypization expenses are therefore expected from the adoption of CAD techniques, aimed at device (as well as process) simulation. Technology-CAD tools are routinely used in IC production and development environments; however, their diffusion within the HEP community is relatively recent, and their use has been mostly restricted to passive device-characterization, such as evaluation of interstrip impedances, leakage currents, etc.

In this paper, the application of numerical device simulation to the analysis of high-resistivity, single-sided silicon microstrip detectors is illustrated; besides carrying out the complete characterization of equivalent-circuit parameters, we present a novel approach to the simulation of sensors' active behavior, i.e., to the analysis of charge collection phenomena. This has been made possible by means of a suitably "customized" transient simulation technique. Details on the actual characteristics of the simulation tool are presented in Sect. 2, with particular emphasis on the features introduced in order to model the charge-collection dynamics.

Simulation results are presented in Sect. 3: here, radiation influence over a couple of important detector-design parameters (namely, the depletion voltage and the strip capacitance) has been evaluated by properly adjusting the oxide charge and the effective doping concentration. Sect. 4 below is more specifically devoted to the analysis of the charge collection mechanisms: the time-domain sensor response to a particle crossing the detector is simulated, from which the spatial resolution is estimated.

Conclusions are eventually drawn in Sect. 5.

2 THE SIMULATION PACKAGE

The analysis has been carried out with HFIELDS (Hybrid FInite-ELement Device Simulator), a device simulator developed at the University of Bologna [1]. It is a general-purpose semiconductor-device analysis package: in the version used for this work, the numerical solution of the classical "drift-diffusion" transport model equations is obtained over a two-dimensional discretized spatial-domain. More specifically, the simulator solves the following set of partial differential equations:

$$\nabla\cdot(-\epsilon_s\,\nabla\varphi) = q(p - n + N) \tag{1}$$

$$\frac{\partial n}{\partial t} - \frac{1}{q}\,\nabla\cdot\vec{J}_n = G - R \tag{2}$$

$$\frac{\partial p}{\partial t} + \frac{1}{q}\,\nabla\cdot\vec{J}_p = G - R \tag{3}$$

consisting of Poisson (1) and carrier-continuity equations for electrons (2) and holes (3). In the above equations the symbols have their usual meaning: namely, φ is the electric potential as well as n and p are the electron and hole concentrations, respectively. The term $(G - R)$ represents the net generation rate per unit volume. Furthermore, in the equation (1), $N = N_D^+ - N_A^-$ accounts for the net ionized impurity concentration, whereas current densities appearing in Eqs. (2,3) are expressed through the customary approximation:

$$\vec{J}_n = q\mu_n\left[-n\nabla\varphi + \frac{k_B T}{q}\nabla n\right] \tag{4}$$

$$\vec{J}_p = q\mu_p\left[-p\nabla\varphi - \frac{k_B T}{q}\nabla p\right] \tag{5}$$

Discretization of Eqs. (1, 2, 3) is carried out over the spatial domain by means of a "finite volume" approach (Box Integration Method, BIM [2]). Such an integration scheme allows for the adoption of an unstructured discretization grid, needed to render the actual device geometry. A triangular mesh is used in the 2D case, which ensures good conformability to irregular contours. Unknown quantities (electric potential φ and carrier concentrations $n,\ p$) are mapped at nodal meshpoints. Equation non-linearity is managed via a Newton-Raphson procedure; time integration of the equations above is obtained by means of backward Euler algorithm. A quite general set of physical models has been incorporated into the code, with particular emphasis on carrier mobility and several generation/recombination mechanisms [3].

Different analysis modes can be exploited: DC, AC and transient simulation algorithms are available. For our specific purposes, DC analysis can be used to estimate static parameters such as the device depletion voltage, interstrip resistance, leakage currents, critical fields, etc. The AC analysis mode allows for predicting interstrip and bulk device capacitances, whereas the transient analysis has been used to investigate charge collection dynamics.

In the latter case, the code has been modified to accomplish radiation-induced electron-hole pairs to be taken into account. We proceed as follows: a generation term, accounting for electron-hole pairs generated by an impinging particle, has been included in the right-hand side of Eqs. (2, 3). Such a term can be arbitrarily distributed in time and space, accounting for the actual trajectory of the ionizing particle. In practice, since the actual duration of collision events is largely negligible with respect to the typical timescale of charge-collection transients, we neglect the detailed dynamics of generation events, and start by distributing a given amount of electron-hole pairs (which can thus include also secondary-generated pairs) along a user-definable path. In the simplest case, a δ-distribution in time is adopted, whereas suitable algorithms are employed to map the initially-generated charge over the discretized spatial domain. In particular, according to the BIM scheme, the charge is lumped at discretization mesh nodes: we first identify the nodal "control volumes" interested by the particle trajectory, then distribute the total amount of generated charge among the related nodes. Charge contributions are weighted by the fraction of the particle path pertaining to each "box", in order to achieve a charge distribution which is independent of the actual discretization mesh. In order to ensure accurate simulation responses, rather stringent mesh constraints are introduced in this phase; to this respect, the "box" size needs to be small, compared to the average charge collection path. The transient simulation then proceeds from this starting condition onward; generated charge travels within the device under the combined action of diffusion and electrostatic forces, until it is collected at device terminals. Self-consistent modeling of details of interest, such as, for instance, charge sharing between adjacent strips, is thus achieved.

Alternative approaches to the analysis of strip charge collection are found in the literature: Monte Carlo calculations have been carried out by Kalbfleisch et al. [4]; according to their approach, the detector is discretized by splitting it into separate "slices" centered on each strip. A constant, vertical field is assumed within each slice, whereas carrier diffusion (i.e., population transitions between adjacent slices) is accounted for by Monte Carlo analysis. After a given drift time, charge pertaining to each slice is eventually integrated to obtain the strip-collected charge.

A more accurate account of actual electric field is given in the approach suggested by Castoldi and Gatti [5], based on a three-dimensional solution of Poisson's equation. By assuming full depletion, electric field can be analytically calculated only at a restricted number of points along the actual carrier trajectory, leading to a quite efficient computational algorithm. In this case, however, diffusion is not self-consistently accounted for.

Ohmic and diffusive transport are accounted for, in a simplified manner, in the work by Sailor et al. [6], whose approach has been subsequently extended in [7] and [8]. Here, the whole set of Eqs. (1, 2, 3) is solved by assuming 1D field profiles, normal to the detector surface, as well as 1D diffusion "planes", parallel to the detector surface.

Our approach differs from the above ones with many respects: since it is based on the self-consistent, fully 2D solution of transport equations, it is not restricted to the analysis of fully-depleted structures, and is therefore suitable for the analysis of heavily irradiated structures. The diffusion and electrostatic forces involved in the charge collection are simultaneously taken into account, without simplifying hypotheses on their distribution. Moreover, the algorithm is integrated within the device-simulation framework, and therefore takes advantage of its embedded features: no simplifying assumption needs to be made about the device geometry, and detailed account of many physical effects can be given at no additional cost.

3 DETECTOR SIMULATION

The simulated structure, shown in Fig. 1, consists of a single sided, DC-coupled detector, featuring 14 μm p^+ strip implantation width and 50 μm pitch. The p-strips doping profile is Gaussian, with parameters extracted from

device measurement and process simulation [9]. Such a detector is built on high-resistivity ($\approx$ 10 KΩ cm), n-doped, 300 μm-thick silicon wafers [10]. Five strips have been considered, thus neglecting the influence of third

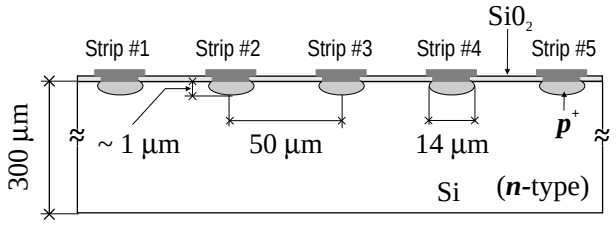

Figure 1: Sketch of the detector structure.

(as well as higher-order) neighbors. A 2D simulation has been carried out, so that fringe effects at strip ends have been neglected as well. The discretization grid adopted for device simulation counts 2200 meshpoints and 4100 triangular elements. Such a grid results from a careful balancing among different (and somehow contrasting) requirements: reliability of the simulation results, as well as the computational cost, are fairly sensitive to the meshpoint distribution. A strongly non-uniform mesh is needed to resolve some details in the μm range (near the strip junctions), avoiding, at the same time, the computational overhead required by an unnecessarily dense mesh in the device bulk and near the backplane. In Fig. 2 the electron concentration at equilibrium is shown: positive charges trapped into the oxide are responsible for the thin electron accumulation layer (visible in the foreground) which develops at the silicon surface, between strip contacts. As demonstrated by Fig. 3, such an accumulation layer is still present even when the detector is fully depleted (i.e. at normal operating conditions), so that it clearly plays a significant role on the interstrip capacitances. In order to estimate such capacitances, a set of AC-analyses

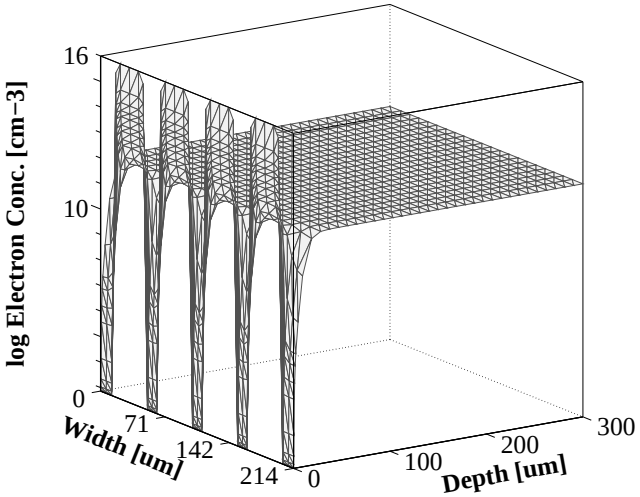

Figure 2: Equilibrium electron concentration.

has been carried out, reproducing a typical measurement set-up: capacitance between a given electrode and the other ones can be individually evaluated by injecting a small signal into the former electrode, at the same time keeping the remaining electrodes at their bias value. This allows us to easily extract some of the basic parameters, such as the depletion voltage and the interstrip capacitance.

The code allows for arbitrary distributions of oxide- and interface-trapped charge to be taken into account, as well as for surface recombination effects: most of these parameters can be correlated to the radiation damage suffered by the detector. Irradiated device behavior can be interpreted by referring to two main damage categories: bulk silicon damage and surface damage. The effect of bulk radiation damage for high resistivity, n-type detector has been extensively studied in recent years ([11], [12]). At first order, bulk radiation-damage can be taken into account by introducing an irradiation-dependent, effective doping-concentration in the substrate N_{eff}. LHC detectors are expected to undergo large radiation doses (in the order of $\sim 1 \times 10^{14}$ particle cm$^-$2), which may drastically alter N_{eff}. Several effects cooperate to the effective-doping variation, which can be summarized as follows [13]:

- donor removal;

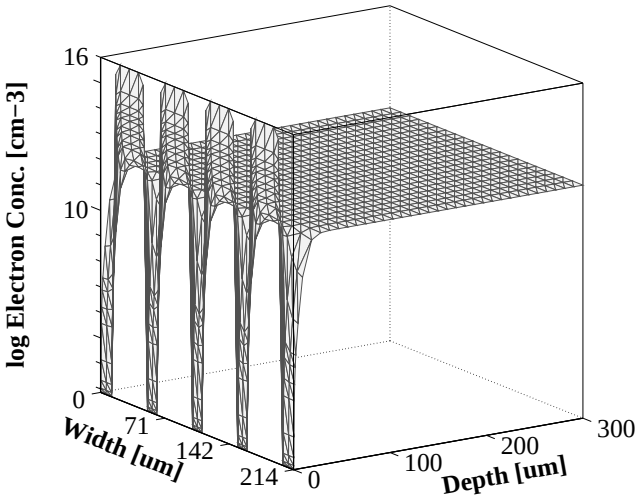

Figure 3: Reverse-bias electron concentration ($V_{bias} = 100$ V).

- acceptor creation;
- creation of defects.

These effects have different and complex causes, a detailed physical discussion of which goes far beyond the scope of this paper; however, by neglecting temperature and time dependent phenomena (i.e. annealing), the effective bulk concentration can be correlate to the irradiation flux ϕ, by means of the following relationship:

$$N_{eff}(\phi) = N_{D,0} \cdot e^{-c\phi} - N_{A,0} - \beta\phi, \tag{6}$$

where $N_{D,0}$ and $N_{A,0}$ are the initial donor and acceptor concentration, respectively, c is the donor removal rate and β is the creation rate of radiation-induced acceptors. Thus, in order to evaluate the bulk-damage influence over device performance, a set of simulation have been carried out, accounting for different values of N_{eff}. For instance, the detector's depletion voltage can be inferred from the $1/C^2$ versus V_{bias} plot shown in Fig. 4. Here, C represents the strip capacitance toward the backplane contact: the "knee" position in the curve indicates the depletion voltage, which decreases with the radiation exposure.

In order to check for simulation consistency, response of an actual detector has been measured: first, by measuring the non-irradiated detector, an effective substrate doping concentration of $N_{eff} = 3.6 \times 10^{11}$ cm^{-3} has been estimated. Then the sample has been exposed to neutron irradiation, up to an integrated fluence of $\phi = 1.0 \times 10^{13}$ n cm^{-2}. Eq. 6 predicts, for such a dose, a lowering of the effective doping N_{eff}. By accounting for the values of c and β reported in [13], a value of 2.0×10^{11} cm^{-3} is worked out, which has been considered for the simulation of the irradiated detector: from Fig. 4, a depletion voltages of 18.5 V is extracted, which well compare with the experimental value of ~ 20 V.

Surface damage, instead, can be taken into account by properly characterizing the oxide-trapped charge and the interface recombination centers. The positive charge localized at the SiO_2 layer, in turn, depends on fixed charge, mobile positive impurity ions and trapped holes: the first two components mostly come from the fabrication process, whereas the hole contribution is sensitive to the irradiation [14].

Let's assume, for the sake of simplicity, that all the trapped charges are localized at the silicon/oxide interface. This typically results in an equivalent surface charge density in the order of 1.0×10^{11} cm^{-2} for the non-irradiated detector, whereas the amount of trapped charge is expected to saturate at 1.0×10^{12} cm^{-2}, even under heavy irradiation condition, for the $[111]$ silicon orientation used in detector fabrication [15].

The SiO_2-embedded positive charge layer causes a thin electron accumulation layer to build-up at the $Si - SiO_2$ interface, as previously highlighted in Figs. 2 and 3. Effects of such a layer on the interstrip capacitances are illustrated by Fig. 5: as expected, the amount of oxide-trapped charge modulates significantly the accumulation interfacial layer, which mostly reflects on the nearest-neighbors capacitance. On the other hand, no appreciable dependency on the amount of oxide-trapped charge is exhibited by the substrate capacitance, so that negligible alteration are induced on the depletion voltage, as confirmed by Fig. 6; the electric field profile along the detector height is in fact scarcely sensitive to the shallow perturbation induced at the surface; the backplane capacitance can thus be basically correlated only to device geometry.

In this case too, results reported in Fig. 5 can be compared with measured values. With reference to the non-irradiated detector, full-depletion capacitances to nearest-neighbors and second-nearest-neighbors of 1.30 pF/cm and 0.25 pF/cm, respectively, are extracted from measurements, whereas simulation predicts values of 1.12 pF/cm and 0.22 pF/cm. The irradiated detector has then been simulated, simultaneously accounting for bulk damage (N_{eff} variation) and surface damage (Q_{ox} variation). Even though only such a first-order account of radiation damage is given, a good agreement is found between simulated results, which allow to estimate an interstrip capacitance of 1.4 pF/cm and 0.24 pF/cm (nearest-neighbors and second-nearest-neighbors, respectively) and the corresponding measured data of 1.5 pF/cm and 0.28 pF/cm.

4 CHARGE COLLECTION AND RESOLUTION ANALYSIS

As introduced in Sect. 1, a transient-analysis numerical algorithm has been devised and implemented, to evaluate charge collection phenomena. A set of simulations has been performed, in which all trajectories are assumed to be perpendicular to the detector surface.

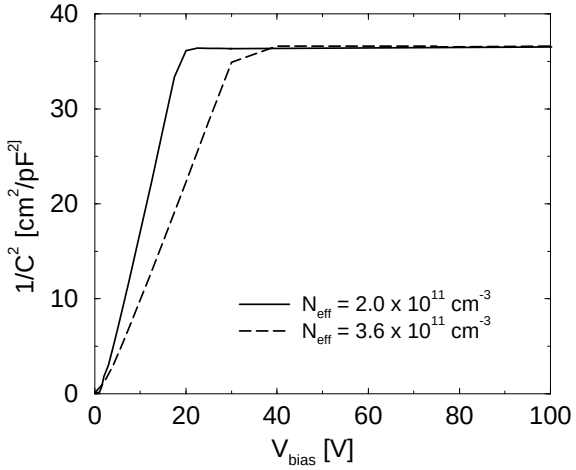

Figure 4: $1/C^2$ plot, from which the depletion voltage can be estimated.

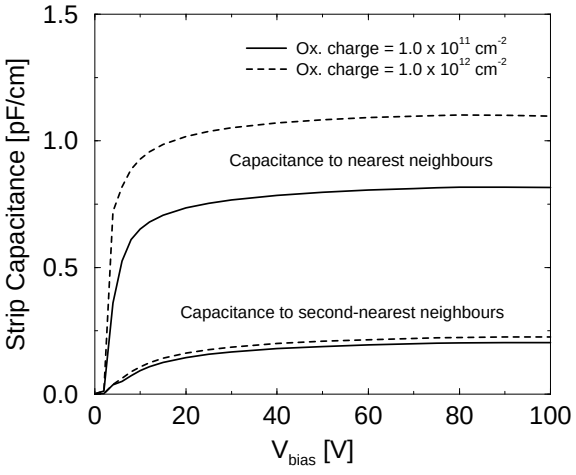

Figure 5: Different contributions to strip capacitance.

A 4-strip subset of the detector has been accounted for in this case and the central region of the discretization grid has been more heavily refined, in order to ensure better spatial resolution of the simulation.

Fig. 7.a shows the hole distribution, for a given trajectory, at the initial time-step of the simulation (i.e., immediately after the charge abrupt generation: 2.4×10^3 electron-hole pairs are uniformly distributed along the trajectory). The

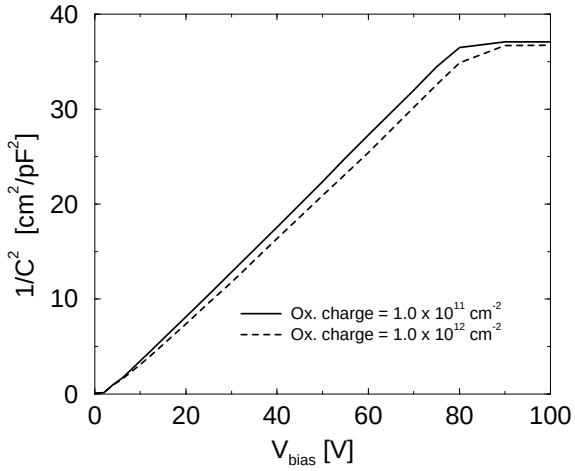

Figure 6: $1/C^2$ plot, depending on the interfacial charge ($N_{eff} = 1.0 \times 10^{12}$ cm^{-3}).

strips are visible in the plot background, whereas the sharp ridge along the surface defines the particle trajectory (in this particular plot, the trajectory crosses the device just in the middle of an interstrip region). This is assumed as the transient simulation initial condition: from this point on, the structure relaxes back toward the steady-state. Fig. 7.b illustrates the same hole concentration after a 30 ns interval: carrier diffusion has smoothen the ridge; the hole flow conveyed toward *p*-strips is also evident. Fig. 7.c is taken after 130 ns: in this case, the concentration ridge is almost completely flattened down, since most of the excess charge has already been drained by the electrodes. Only a wide tail of charges remains visible; at this time, deep-bulk concentration has already recovered its original value.

Strip-collected currents are illustrated in Fig. 8, referring to both the irradiated and the non-irradiated detector. Such predictions well compare with published data [16, 17, 18]. To this regard, it should be mentioned that in this set of simulation no load was assumed to terminate the strips: smoother current peaks should have been obtained if a reactive load were connected, accounting for the finite shaping time of the read-out amplifier. Nevertheless, charge sharing between strips is correctly predicted, the relative peak amplitudes matching those reported in [17].

Differences between the two sets of curves can be ascribed to the effective doping decreases due to irradiation. This, in turn, reduces the electric field; lateral current spreading, due to carrier diffusion, therefore becomes relatively more significant, leading to an increase of the outer-strip currents.

Then, a detailed analysis of the correlation between the particle trajectory and the detector response has been carried out, in order to extract relevant design information, such as the spatial resolution allowed by the detector itself.

A number of simulations have been carried out, accounting for different trajectories, which spans over the space between the two inner strips. Fig. 9 shows the amount of charge collected by each of the inner strips, depending on the impact position of the particle. In order to get realistic estimates, however, some account should be given for a number of non-idealities of the actual detector. First, the simulation presently accounts for a uniform generation rate along the trajectory, whereas rather large fluctuations around such an average value are expected within real devices, described by a Landau distribution. Moreover, some Gaussian noise comes from the front-end electronics: an equivalent electronic noise-charge of 0.2 fC is obtained by testing a LHC-like front-end electronics (40 ns shaping time) coupled to a 12cm-long detector module.

Such effects can be accounted for by means of two different smearings, which are applied to the simulated data. The charge collected at each strip in the cluster is smeared *i)* by a Landau distribution, having width $\Gamma_{Landau} = 0.14$ fC and, *ii)* by a Gaussian distribution with $\sigma_{Gauss} = 0.2$ fC. Smearing parameters have been consistently chosen in order to reproduce the typical cluster charge distribution of a single-side microstrip detector, having a peak-charge value at 4 fC and a signal-to noise ratio $S/N = 20$. A cluster is defined, made by the inner strip pair; the cluster-collected charge distribution is shown in Fig. 10; the curve is fitted by a convolution of a Gaussian and a Landau distribution. The η-function, defined as

$$\eta = \frac{Q_{right}}{Q_{left} + Q_{right}} \tag{7}$$

is plotted in Fig. 11, as calculated from the distribution of the collected charge. In Eq. 7, Q_{left} and Q_{right} refer to the charge collected at the left inner strip and at the right inner strip, respectively. The average impact point x_m, for a given value of η, can be obtained by the well-known relation:

$$x_m = \frac{\Delta}{N_0} \int_0^{\eta} \frac{\mathrm{d}N}{\mathrm{d}\eta} \mathrm{d}\eta. \tag{8}$$

In the above equation , N_0 particles, uniformly distributed over x, are assumed to traverse the interstrip gap, which features a $\Delta = 50 \mu m$ pitch. In Fig. 12 the integrated η-function is given, making the relationship between η and the impact position explicit. Eventually, the resolution function of the detector can be evaluated by comparing the generated and estimated (x_m) impact position. In Fig. 13 a Gaussian fit of the resolution function is shown, from which a standard deviation (i.e., the actual detector resolution) of 6.17 μm is obtained, the experimental finding being close to 7 μm.

5 CONCLUSIONS

In this paper, the application of the general-purpose device simulator HFIELDS to the analysis of silicon microstrip detectors has been described: distributed modeling of silicon detectors allows for comprehensive and physically-sound insight of detailed device behavior, thus helping to investigate device-performance sensitivity to both fabrication and environmental parameters.

Simulation results have been validated by comparison with experimental measurements; first-order account of radiation damage has also been introduced into the simulation: future work includes more extensive application of the proposed approach to radiation-tolerance studies.

A novel simulation scheme has been proposed, based on a modified transient-analysis algorithm, and has been employed to analyze charge collection dynamics. Such an approach self-consistently accounts for the motion of impact-generated carriers, and does not require simplifying assumptions typical of alternative methods. Raw simulation results have been post-processed, in order to extract realistic estimates of the detector spatial resolution.

A straightforward link between device simulation and physically-relevant performances can thus be established, proving the usefulness and the practicality of numerical device simulation as an aid for silicon microstrip detector design and optimization.

References

[1] G. Baccarani, P. Ciampolini and A. Pierantoni, “Three-dimensional simulation of semiconductor devices: state of the art and prospects,” *Nucl. Instr. and Meth.*, vol. A326, pp. 253-259, 1993.

[2] R. Varga, Matrix Iterative Analysis, Prentice Hall, Englewood Cliffs, 1962.

[3] G. Baccarani, M. Rudan, R. Guerrieri and P. Ciampolini, “Physical Models for numerical device simulation,” *Process and Device Modeling*, W.L. Engl ed., North Holland, Amsterdam, 1986, pp. 107-159.

[4] G.R. Kalbfleisch, E.H. Smith, D.H. Kaplan, P. Gutierrez, J. Kuehler, P. Skubic, M. Wood, T. McMahon, J.M. Snow, M. Bullough, A.D. Lucas and C.D. Wilburn, “Charge sharing and resolution studies of double-sided silicon microstripe detectors with boron spray implants,” *Nucl. Instr. and Meth.*, vol. A355, pp. 366-385, 1995.

[5] A.Castoldi and E.Gatti, “Fast tools for 3-D design problems in semiconductor detectors,” *Nucl. Instr. and Meth.*, vol. A377, pp. 381-386, 1996.

[6] W.C. Sailor, H.-J. Ziock, W.W. Kinnison and K. Holzscheiter, “A model for the performance of silicon microstrip detectors,” *Nucl. Instr. and Meth.*, vol. A303, pp. 285-297, 1991.

[7] J. Leslie, A. Seiden, Y. Unno, “Signal Simulations for Double-sided Silicon Strip Detectors,” *IEEE Trans. On Nucl. Sc.*, Vol. 40, No. 4, pp. 557-562, August 1993.

[8] K. Ing, T. Kurosky, R. Johnson and R. Rennels, “Charge Collection in Silicon Strip Detectors with a large strip pitch,” *Proc. of IEEE NSS 94*, Norfolk, VA, Oct. 30, 1994.

[9] R. Della Marina, D. Passeri, P. Ciampolini and G.M. Bilei, ”Silicon Strips Detectors for LHC: comprehensive process and device analysis,” *4th International Conference on Position Sensitive Detectors*, Manchester, 1996.

[10] G. Tonelli, E. Focardi and R.J. Wheadon, "Double-sided radiation-resistant microstrip detectors: technology and results," *Nucl. Instr. and Meth.*, vol. A377, pp. 422-428, 1996.

[11] J.A.J. Matthews, P. Berduis, M. Frautschi, H. Sadrozinski, K. O'Shaughnessy, L. Spiegel, A. Palounek, H. Ziock, N. Bacchetta, D. Bisello, A. Giraldo, "Bulk radiation damage in silicon detectors and implications for LHC experiments," to be published in *Nucl. Instr. and Meth. in Phys. Res. A.*

[12] B. Dezillie, F. Lemeilleur, M. Glaser, G.L. Casse, "Experimental results on radiation-induced bulk damage effects in float-zone and epitaxial silicon detector," *Int. Workshop on Vertex Detectors*, Cagliari, Italy, 1996.

[13] S.J. Bates, B. Dezillie, C. Furetta, M. Glaser, F. Lemeilleur, "Proton irradiation of silicon detectors with different resistivities," *Proc. of RADECS'95*, Arcachon, 1995.

[14] C. Leroy, M. Glaser, E.H.M. Heijne, P. Jarron, F. Lemeilleur, J. Rioux, C. Soave, I. Trigger, "Study of the electrical properties and charge collection of silicon detectors under neutron, proton and gamma irradiations," *Proc. of IV Int. Conf. on Calorimetry in High-Energy Physics*, La Biodola, Italy, 1993.

[15] E.H. Nicollian and J.R. Brews, "Radiation effect in $Si0_2$," *MOS Physics and Technology*, Wiley, 1981.

[16] R. Sonnenblick, N. Cartiglia, B. Hubbard, J. Leslie, H.F.-W. Sadrozinski and T. Schalk, "Electrostatic simulations for the design of silicon strip detectors and front-end electronics," *Nucl. Instr. and Meth.*, vol. A310, pp. 189-191, 1991.

[17] N. Bacchetta, D. Bisello, C. Calgarotto, A. Candelori and A. Paccagnella, "A SPICE Model for Si Microstrip Detectors and Read-out Electronics," *IEEE Trans. On Nucl. Sc.*, Vol. 43, No. 3, pp. 1213-1219, June 1996.

[18] H.W. Kraner, Z. Li and E. Fretwurst, "The use of the signal current pulse shape to study the internal electric field profile and trapping effects in neutron damaged silicon detectors", *Nucl. Instr. and Meth.*, vol. A326, pp. 350-356, 1993.

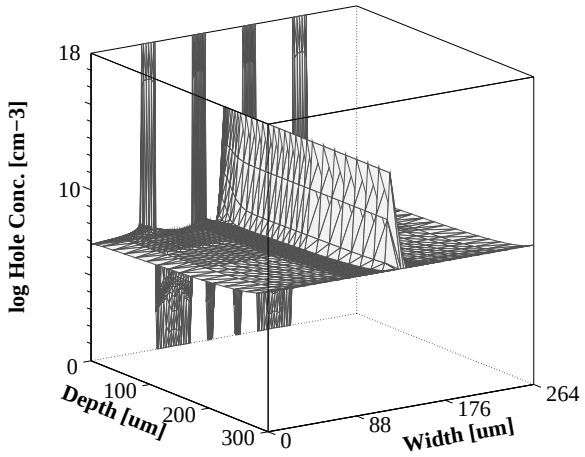

(a): $t = 0$

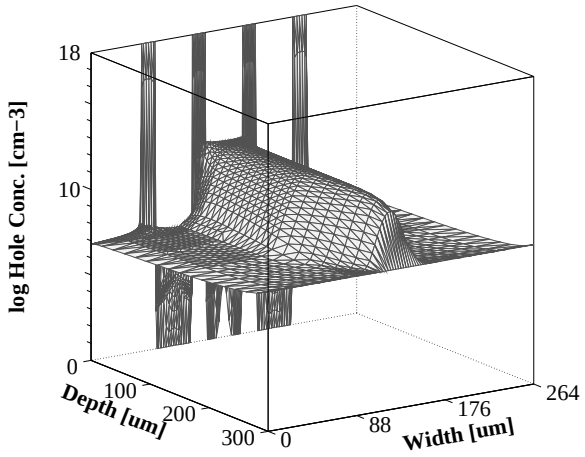

(b): $t = 30$ ns

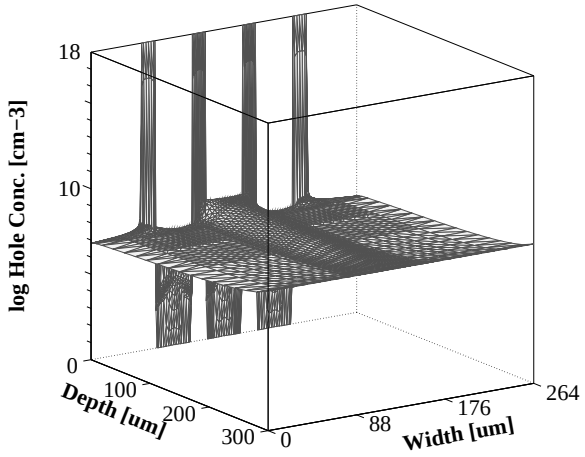

(c): $t = 130$ ns

Figure 7: Transient hole distribution.

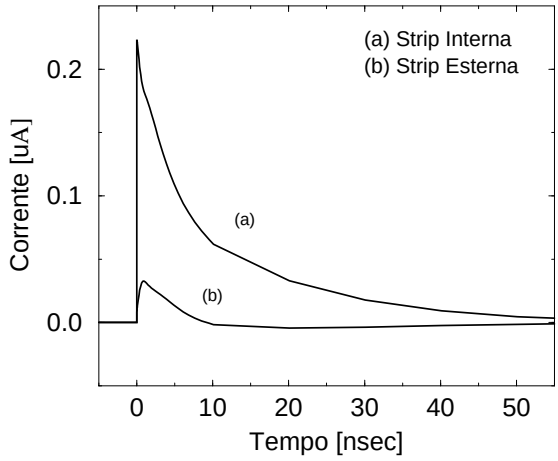

Figure 8: Simulated current pulses, at the inner (a) and outer (b) strips ($V_{bias} = 100$ V).

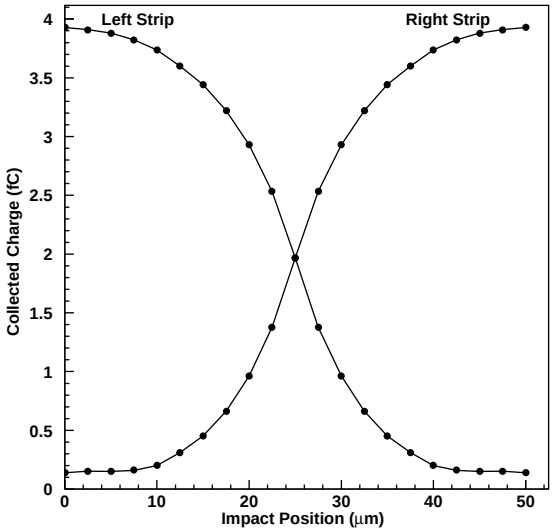

Figure 9: Strip-collected charge, depending on the impact position.

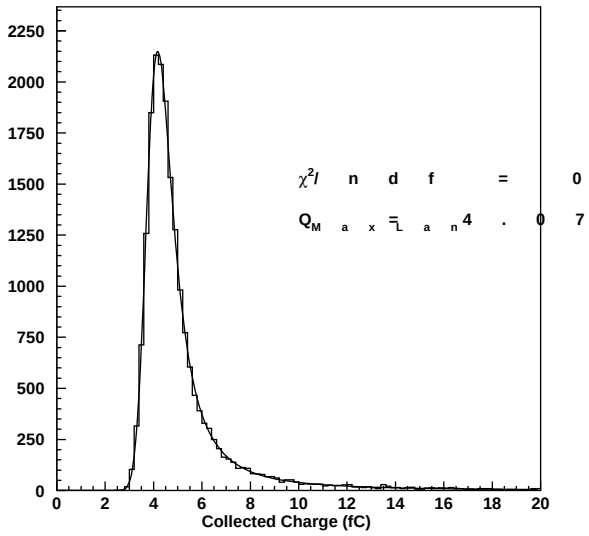

Figure 10: Collected charge distribution.

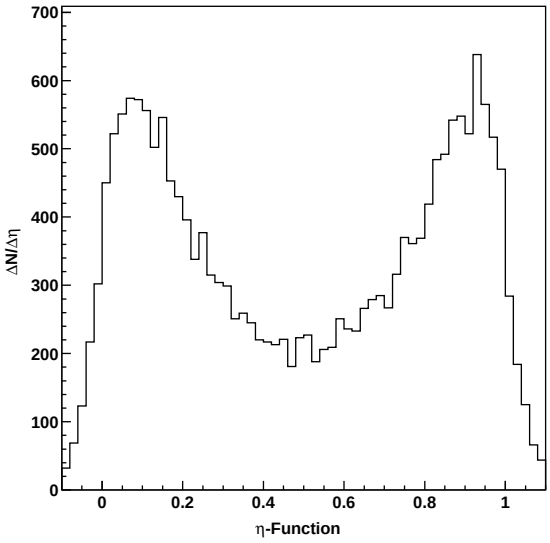

Figure 11: Distribution of the η-function.

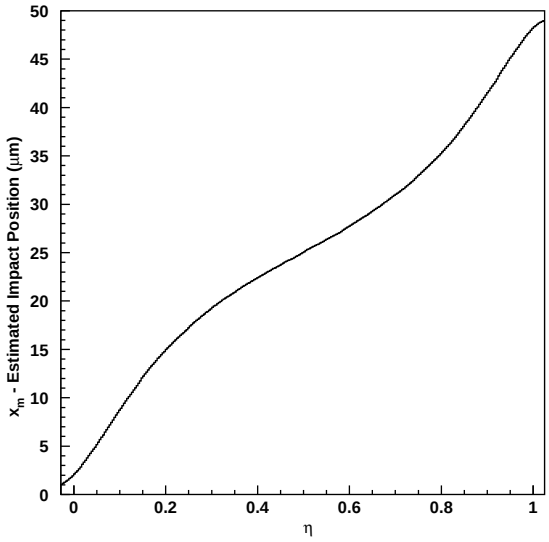

Figure 12: Integrated η-function.

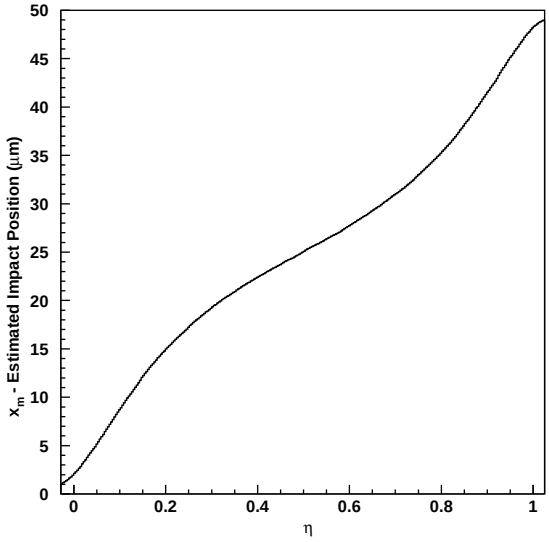

Figure 13: Distribution of the spatial-resolution function.